Electronic Supplementary Information (ESI)

Ultrafine-grained Ni-rich layered cathode for advanced Li-ion batteries

Geon-Tae Park,[a] Dae Ro Yoon,[a] Un-Hyuck Kim,[a] Been Namkoong,[a] Junghwa Lee,[b] Melody M. Wang,[b] Andrew C. Lee,[b] X. Wendy Gu,[c] William C. Chueh,[b] Chong S. Yoon,*[d] and Yang-Kook Sun*[a]

[a] Department of Energy Engineering, Hanyang University, Seoul 04763, South Korea.

[b] Department of Materials Science and Engineering, Stanford University, Stanford, California 94305, United States.

[c] Department of Mechanical Engineering, Stanford University, Stanford, California 94305, United States.

[d] Department of Materials Science and Engineering, Hanyang University, Seoul 04763, South Korea.

Corresponding author: csyoon@hanyang.ac.kr, yksun@hanyang.ac.kr.

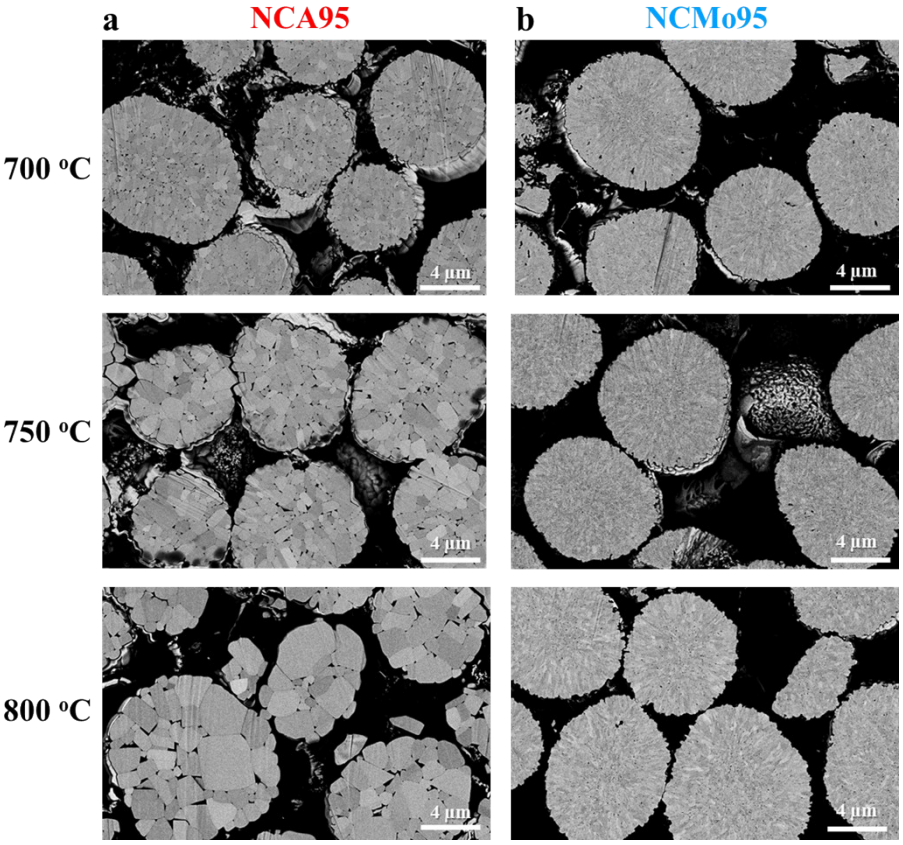

Fig. S1. Low-magnification cross-sectional SEM images of (a) NCA95 and (b) NCMo95 cathodes lithiated at 700, 750, and 800 °C for 10 h.

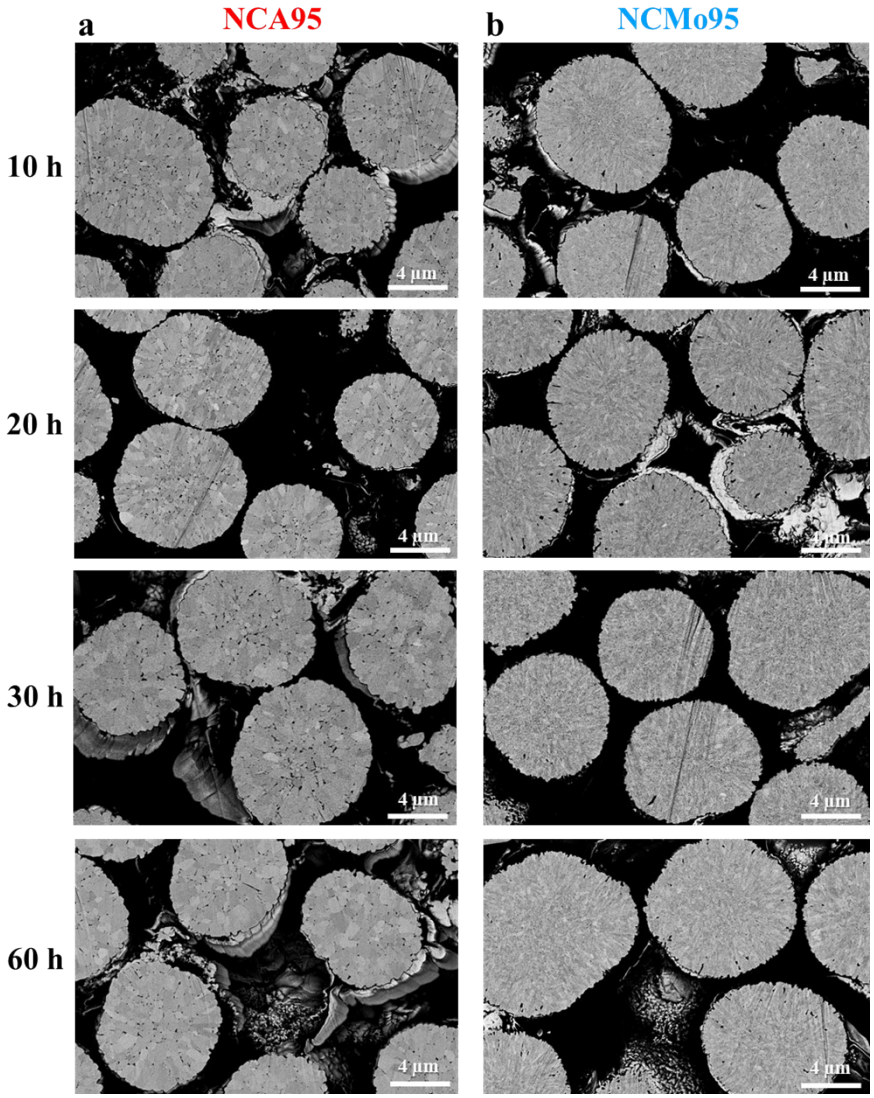

Fig. S2. Low-magnification cross-sectional SEM images of (a) NCA95 and (b) NCMo95 cathodes lithiated at 700 °C for 10, 20, 30, and 60 h.

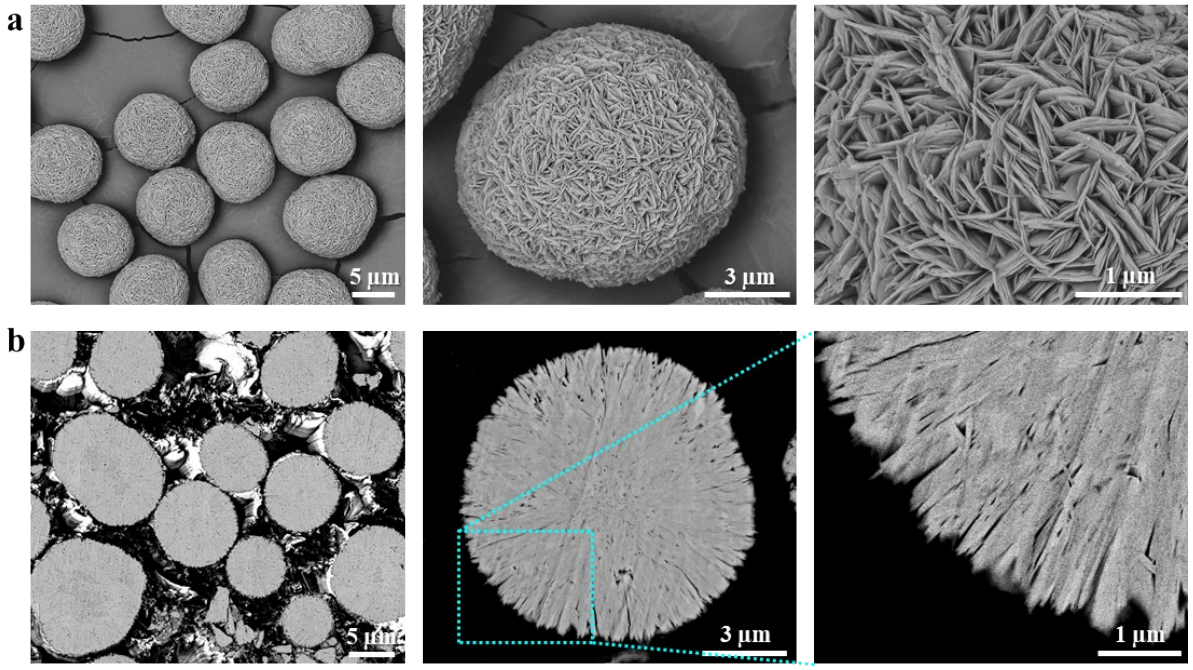

Fig. S3. (a) Surface and (b) cross-sectional SEM images of $[Ni_{0.96}Co_{0.04}](OH)_2$ precursor.

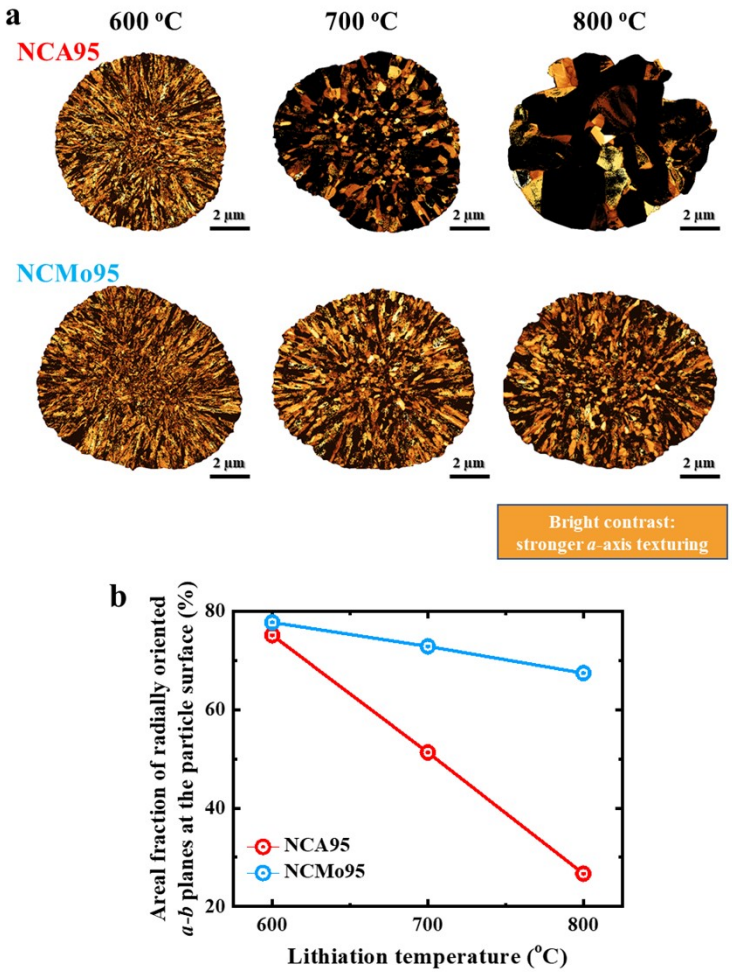

Fig. S4. Orientation of primary particles as a function of lithiation temperature. (a) ASTAR images and (b) areal fraction of radially oriented *a*-*b* planes at the particle surfaces (within 3 μm from the surface) of NCA95 and NCMo95 cathode particles lithiated at 600, 700, and 800 °C for 10 h, indicating that the *a*-*b* plane orientation of primary particles decreases with increasing lithiation temperature.

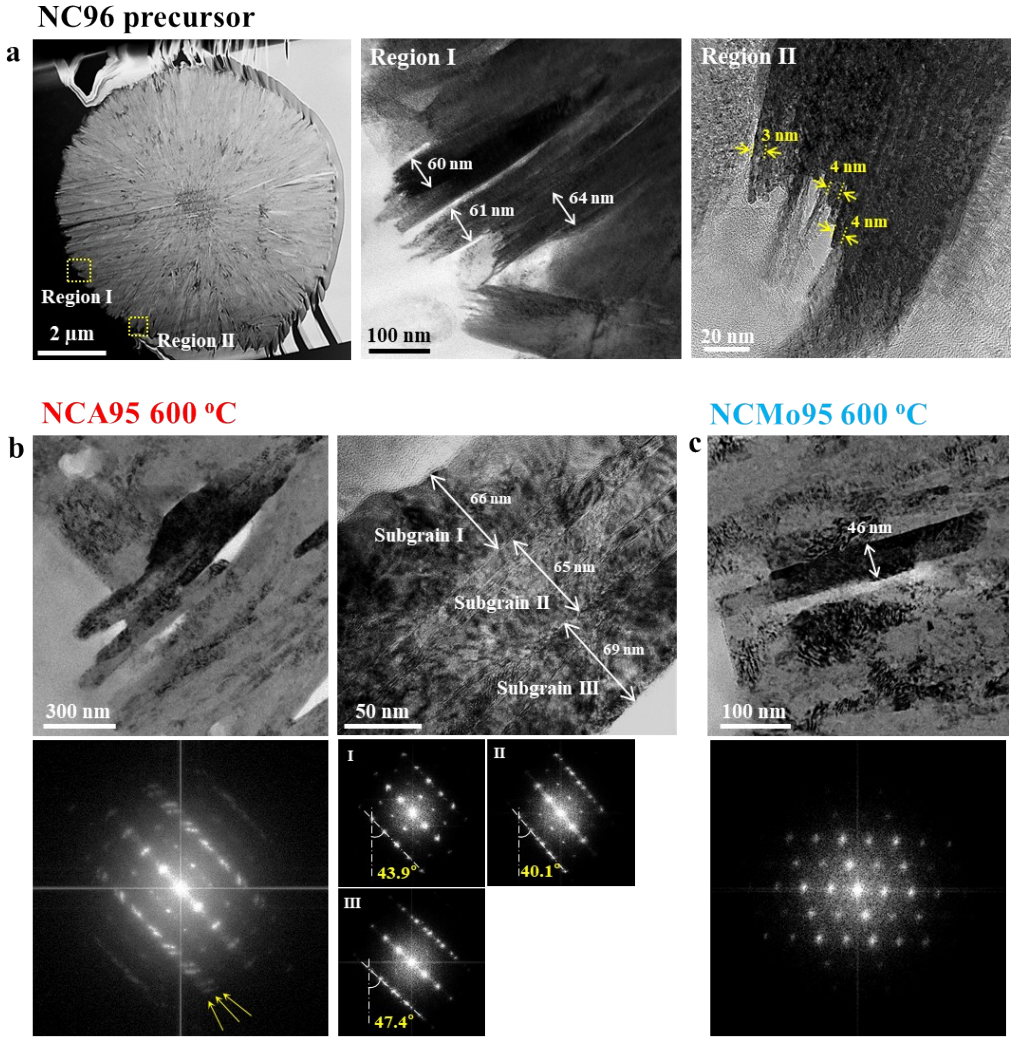

Fig. S5. Coarsening of $[Ni_{0.96}Co_{0.04}](OH)_2$ primary particles under high-temperature lithiation (evolution of NCA95 and NCMo95 primary particles). (a) Dark-field STEM image and high-magnification TEM images (Region I and II) of $[Ni_{0.96}Co_{0.04}](OH)_2$ precursor. Bright-field, high-resolution TEM image and corresponding fast Fourier transform (FFT) of (b) NCA95 (including an SAED pattern) and (c) NCMo95 lithiated at 600 °C for 10 h.

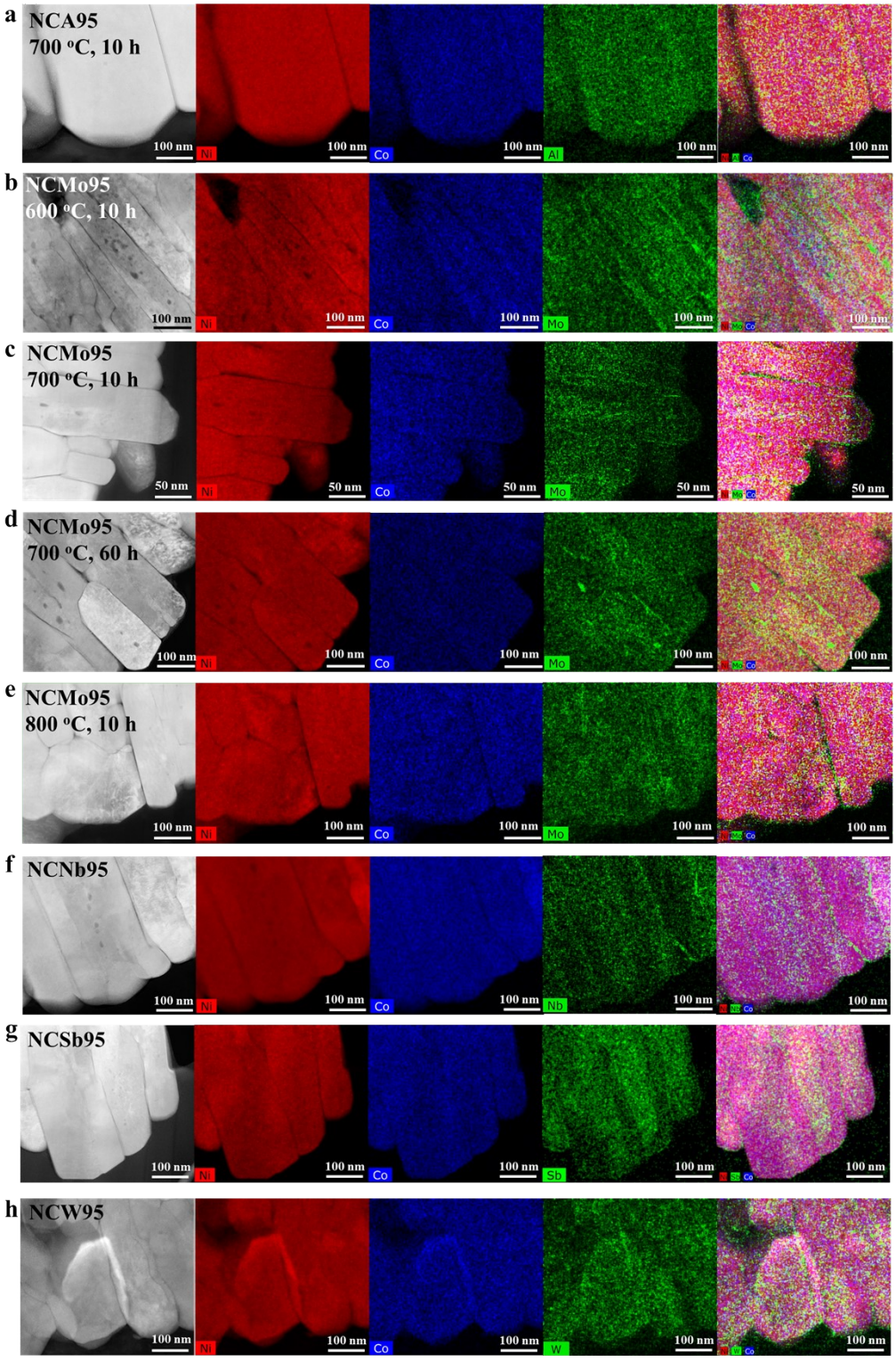

Fig. S6. TEM-EDX elemental maps of an (a) NCA95 cathode lithiated at 700 °C for 10 h; NCMo95 cathode lithiated at (b) 600 °C for 10 h, (c) 700 °C for 10 h, (d) 700 °C for 60 h, and (e) 800 °C for 10 h; (f) NCNb95 lithiated at 700 °C for 10 h; (g) NCSb95 lithiated at 700 °C for 10 h; and (h) NCW95 lithiated at 700 °C for 10 h. This figure illustrates the segregation of sintering inhibitor dopants (Mo, Nb, Sb, W) at cathode grain boundaries.

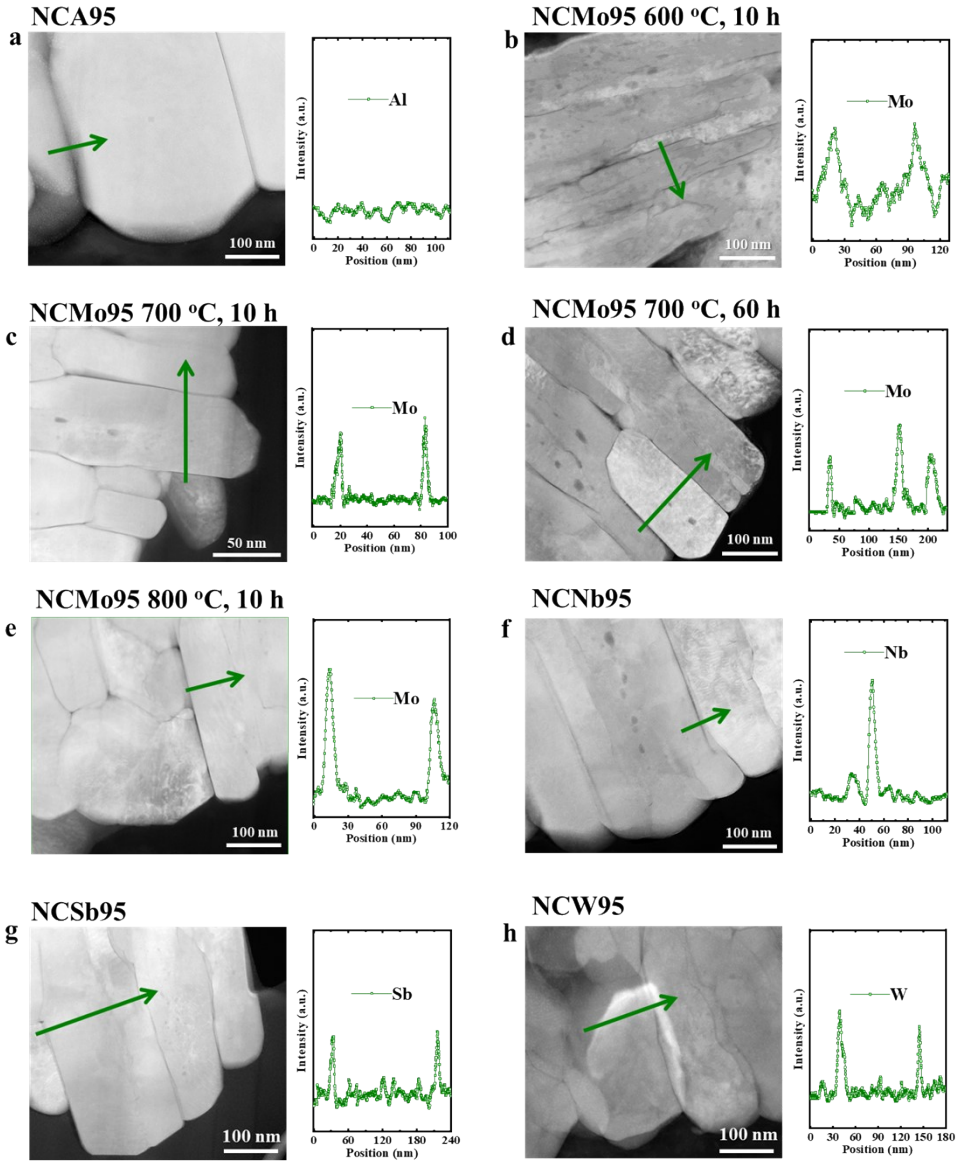

Fig. S7. TEM-EDX elemental line spectra (right) and corresponding dark-field STEM images (left) of (a) NCA95 lithiated at 700 °C for 10 h; NCMo95 lithiated at (b) 600 °C for 10 h, (c) 700 °C for 10 h, (d) 700 °C for 60 h, and (e) 800 °C for 10 h; (f) NCNb95 lithiated at 700 °C for 10 h; (g) NCSb95 lithiated at 700 °C for 10 h; and (h) NCW95 lithiated at 700 °C for 10 h. This figure illustrates the segregation of sintering inhibitor dopants (Mo, Nb, Sb, W) at cathode grain boundaries.

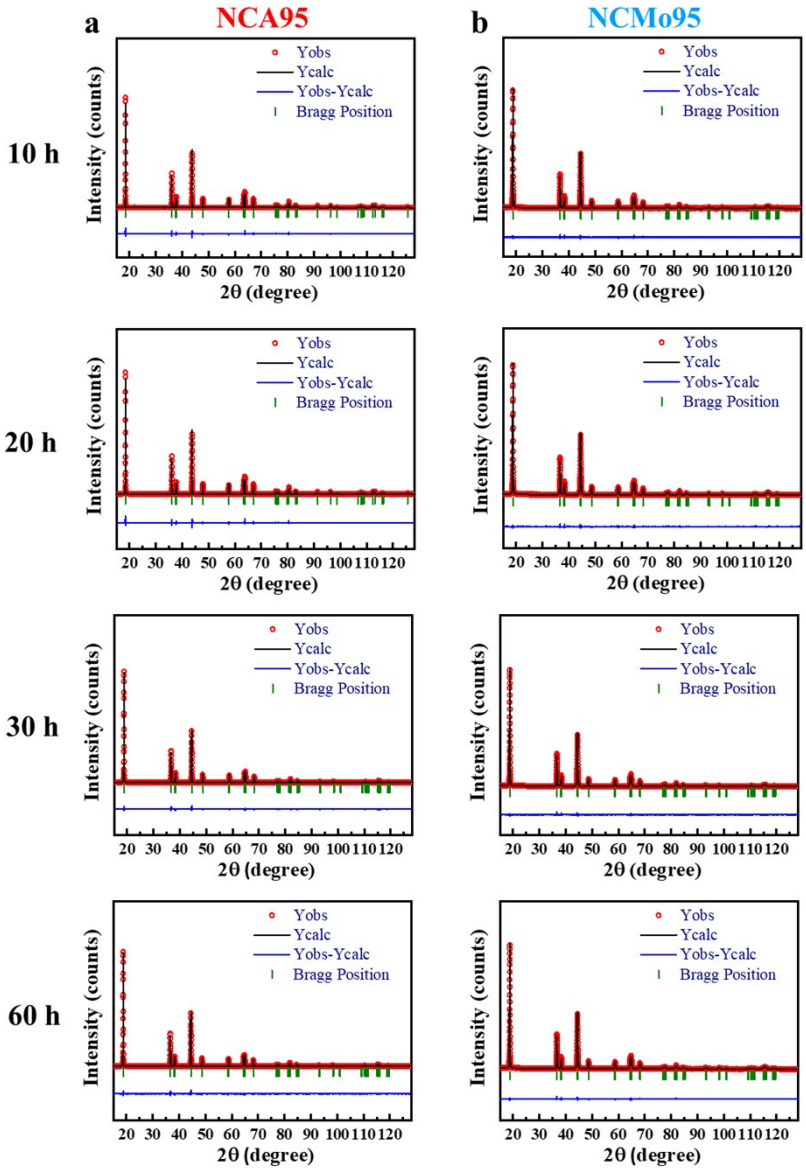

Fig. S8. Rietveld refinement results for (a) NCA95 and (b) NCMo95 cathodes lithiated at 700 °C for 10, 20, 30, and 60 h.

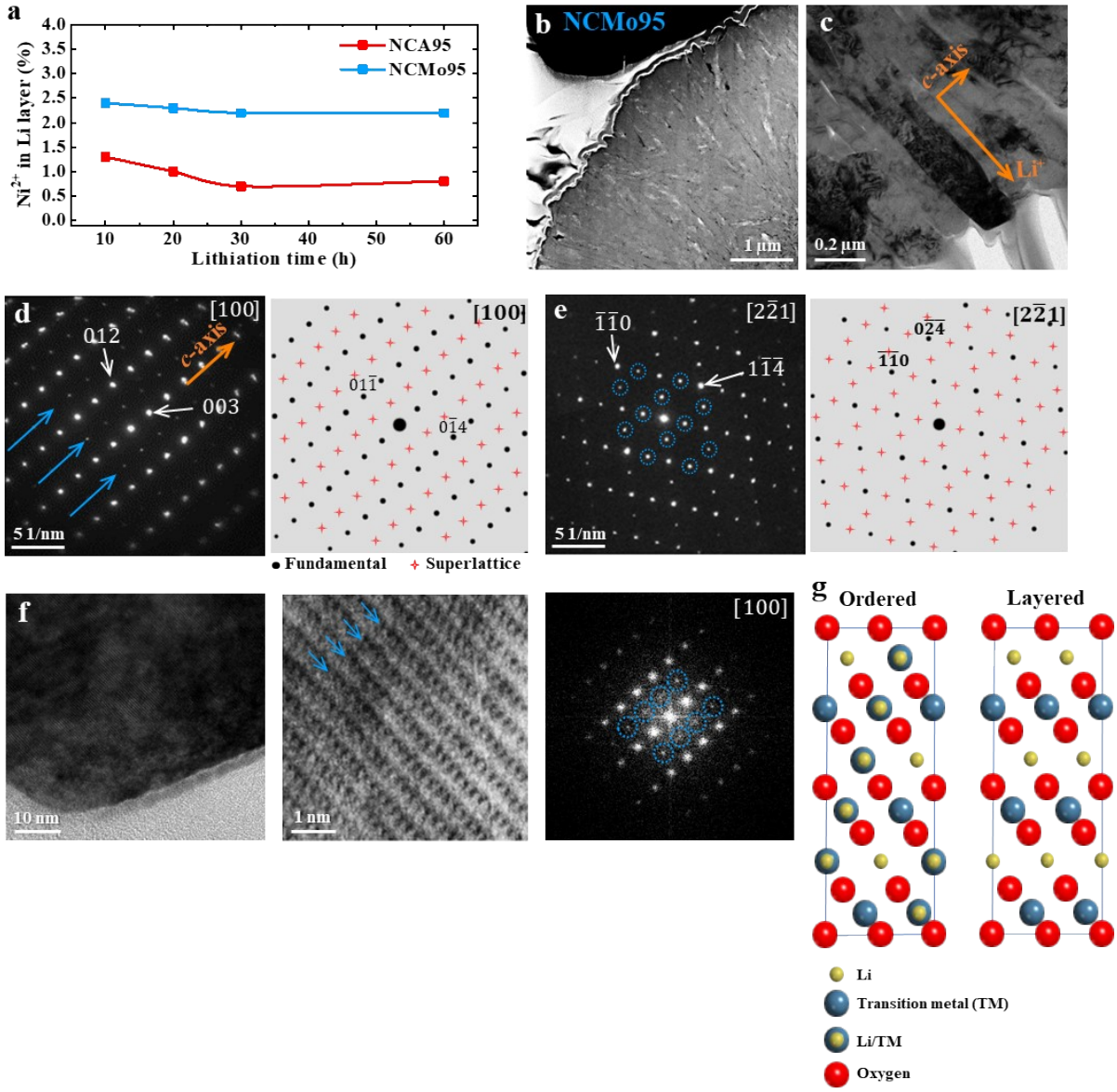

Fig. S9. Li/TM cation–ordered structure and secondary phase observed for a NCMo95 cathode lithiated at 700 °C for 10 h. (a) Percentage of Ni^{2+} in the Li layer of NCA95 and NCMo95 cathodes lithiated for 10, 20, 30, and 60 h. (b) Dark-field cross-sectional STEM image of an NCMo95 cathode and (c) high-magnification TEM image of an elongated primary particle of an NCMo95 cathode. SAED pattern (left) and simulated diffraction patterns along the (d) [100] and (e) [$2\bar{2}1$] zone axes (right) of a Li/TM cation–ordered structure (superlattice spots distinct from the normal layered structure are marked in blue and red). (f) HR and HAADF TEM images together with a fast Fourier transform of the NCMo95 primary particle from (c). (g) Schematic image of Li/TM cation-ordered structure and normal layered structure.

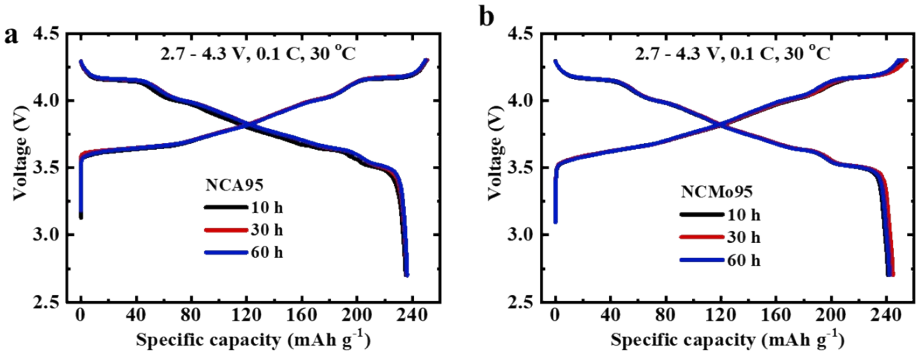

Fig. S10. Initial charge–discharge curves of half-cells cycled at 0.1 C and 30 °C in the voltage range of 2.7–4.3 V, featuring (a) NCA95 and (b) NCMo95 cathodes lithiated at 700 °C for 10, 30, and 60 h.

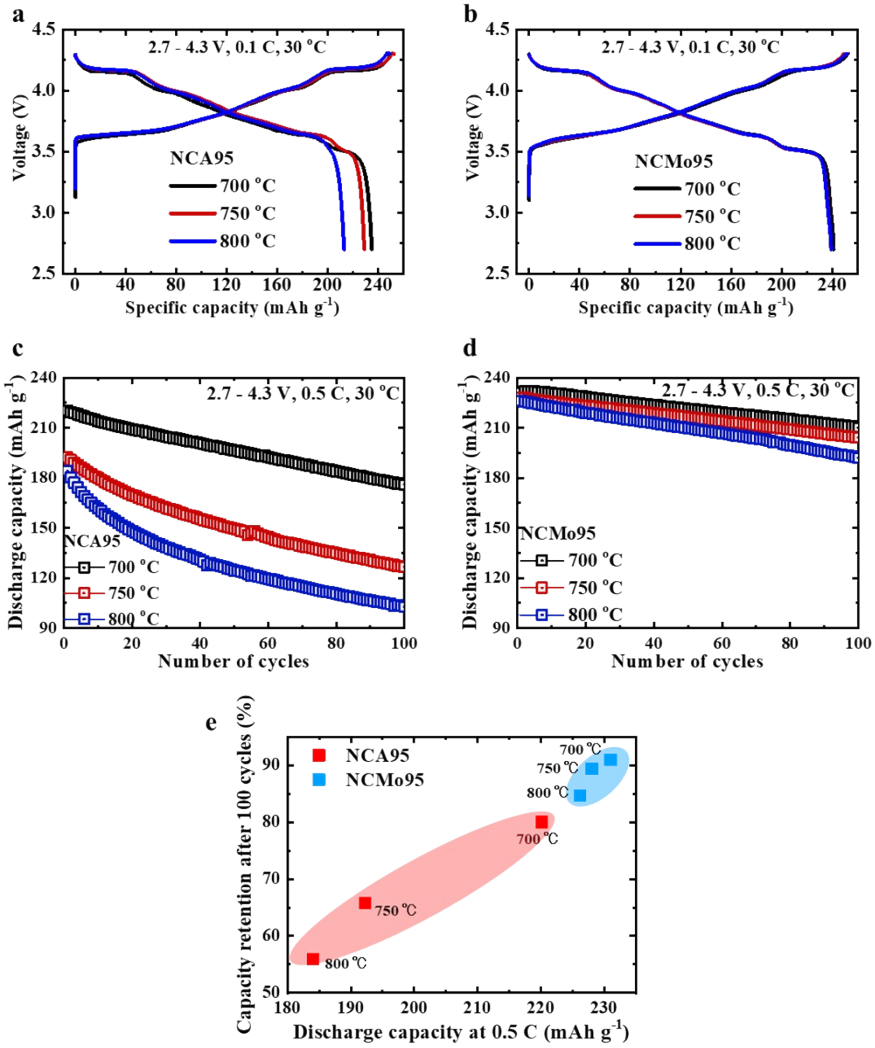

Fig. S11. Initial charge–discharge characteristics of half-cells cycled at 0.1 C and 30 °C in the range of 2.7–4.3 V featuring (a) NCA95 and (b) NCMo95 cathodes lithiated at 700, 750, and 800 °C for 10 h. Cycling performance (at 0.5 C) of the (c) NCA95 and (d) NCMo95 cathodes lithiated at 700, 750, 800 °C for 10 h. (e) Plot of the capacity retention after 100 cycles versus discharge capacity (at 0.5 C) for NCA95 and NCMo95 cathodes lithiated at various temperatures.

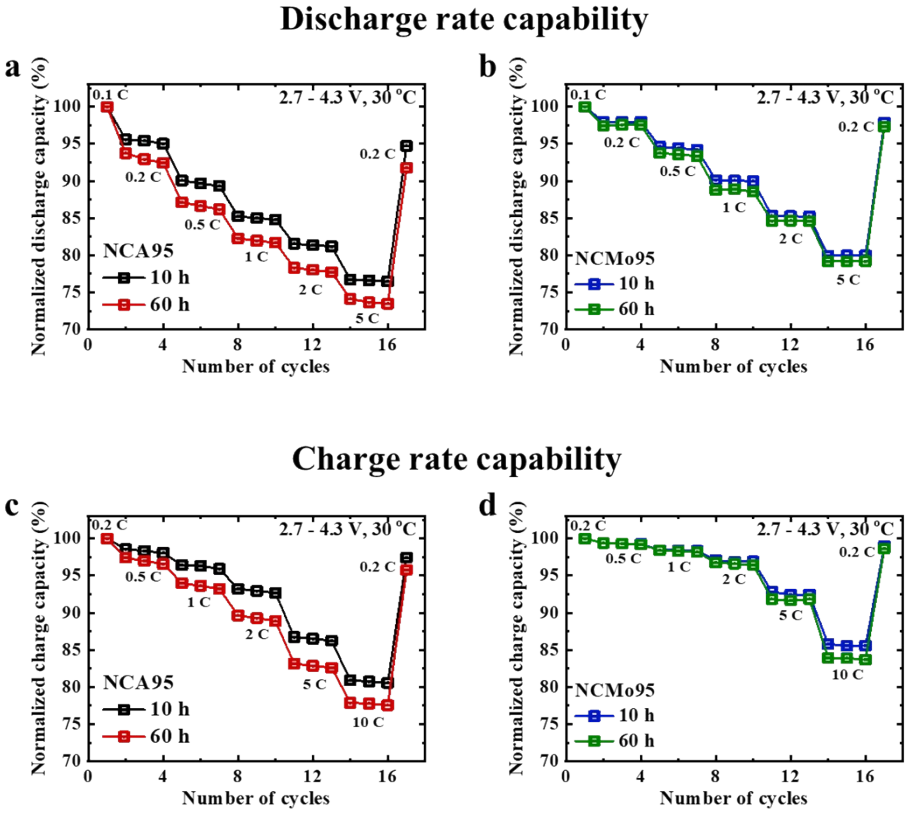

Fig. S12. Comparison of the discharge rate capabilities of half-cells featuring (a) NCA95 and (b) NCMo95 cathodes lithiated at 700 °C for 10 and 60 h. Comparison of the charge rate capabilities of half-cells featuring (c) NCA95 and (d) NCMo95 cathodes lithiated at 700 °C for 10 and 60 h.

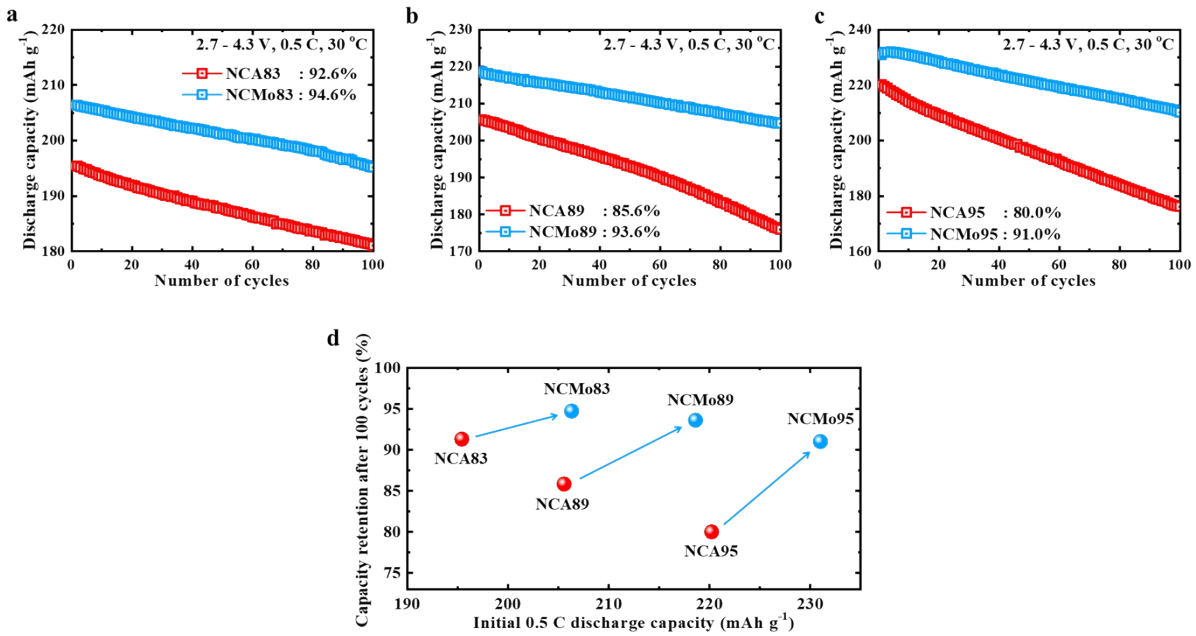

1

2 **Fig. S13.** Comparisons of the cycling performances (at 0.5 C) of half-cells featuring (a) NCA83 and
3 NCMo83 cathodes, (b) NCA89 and NCMo89 cathodes, and (c) NCA95 and NCMo95 cathodes. (d)
4 Initial 0.5 C discharge capacity (at 0.5 C) versus cycle life achieved by various Ni-rich cathodes.

5

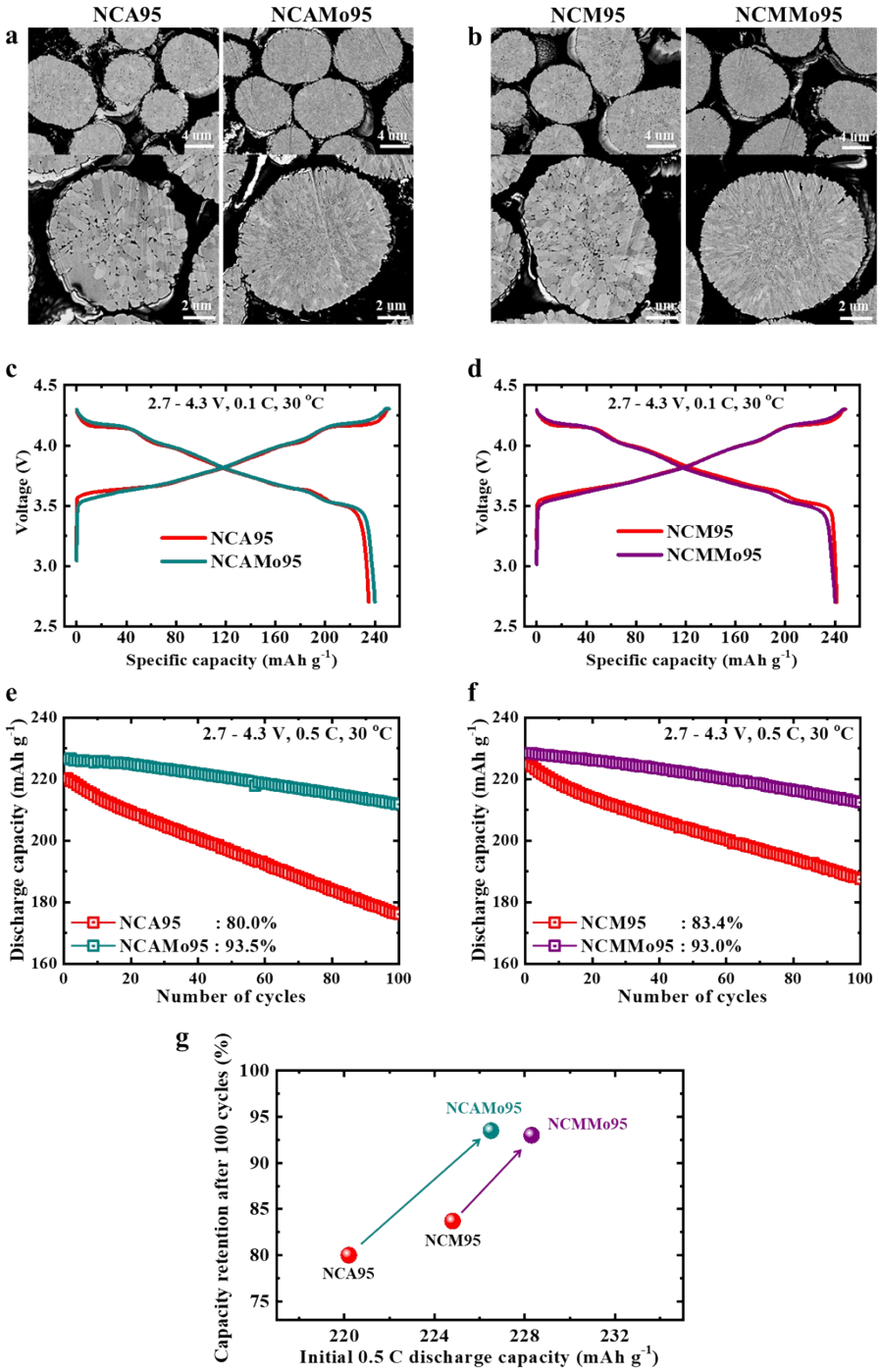

Fig. S14. Low-magnification cross-sectional SEM images of (a) NCA95, $Li[Ni_{0.94}Co_{0.04}Al_{0.01}Mo_{0.01}]O_2$ (hereinafter denoted as NCAMo95) and (b) NCM95, $Li[Ni_{0.94}Co_{0.03}Mn_{0.02}Mo_{0.01}]O_2$ (hereinafter denoted as NCMMo95) cathodes lithiated at 700 °C for 10 h. Initial charge–discharge characteristics of half-cells cycled at 0.1 C and 30 °C in the range of 2.7–4.3 V featuring (c) NCA95, NCAMo95 and (d) NCM95, NCMMo95 cathodes lithiated at 700 °C for 10 h. Cycling performance (at 0.5 C) of the (e) NCA95, NCAMo95 and (f) NCM95, NCMMo95 cathodes lithiated at 700 °C for 10 h. (g) Initial 0.5 C discharge capacity versus cycle life achieved by various Ni-rich cathodes.

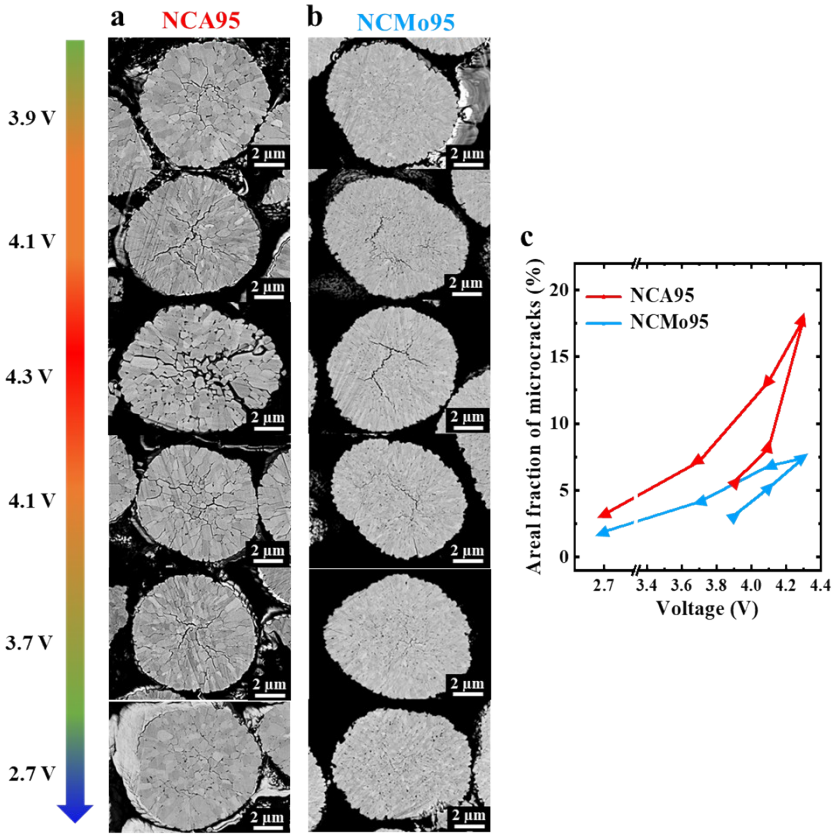

Fig. S15. Comparison of the cross-sectional SEM images of (a) NCA95 and (b) NCMo95 cathodes in various states of charge (charged states: 3.9, 4.1, and 4.3 V; and discharged states: 4.1, 3.7, and 2.7 V during initial cycles). (c) Comparison of the degree of microcracking of NCA95 and NCMo95 cathodes as a function of cell voltage during initial cycles. The cathodes were lithiated at 700 °C for 10 h.

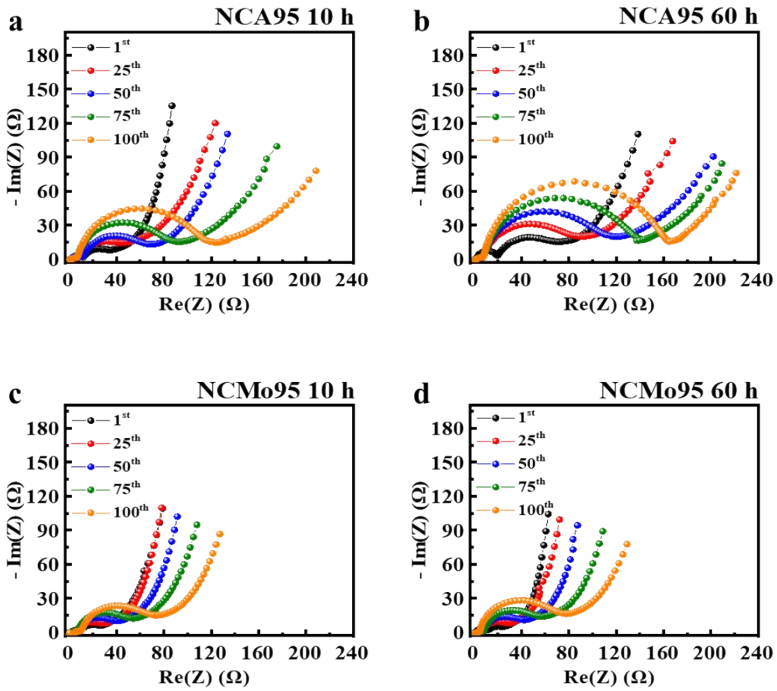

Fig. S16. Nyquist plots of the electrochemical impedances measured every 25 cycles for the NCA95 and NCMo95 cathodes subjected to different lithiation times. NCA95 lithiated at 700 °C for (a) 10 and (b) 60 h. NCMo95 lithiated at 700 °C for (c) 10 and (d) 60 h.

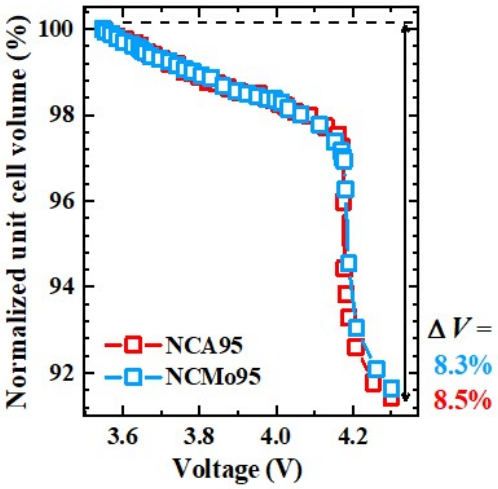

Fig. S17. Comparison of the unit cell volume changes for NCA95 and NCMo95 cathodes during the first charge measured by *in situ* XRD. The cathodes were lithiated at 700 °C for 10 h.

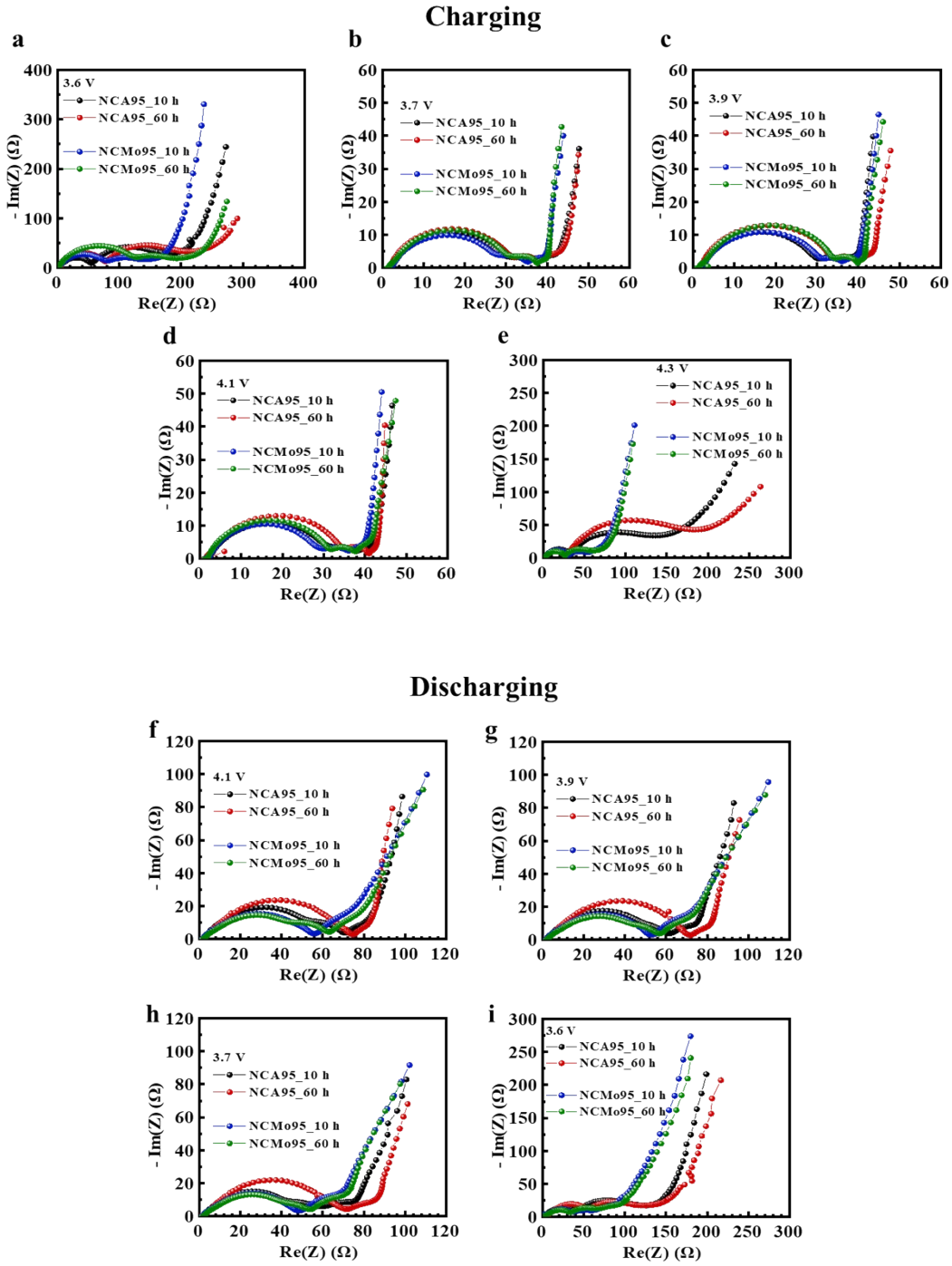

Fig. S18. Nyquist plots of NCA95 and NCMo95 cathodes (subjected to different lithiation times) in various states of charge (charged states: (a) 3.6, (b) 3.7, (c) 3.9, (d) 4.1, and (e) 4.3 V; and discharged states: (f) 4.1, (g) 3.9, (h) 3.7, and (i) 3.6 V).

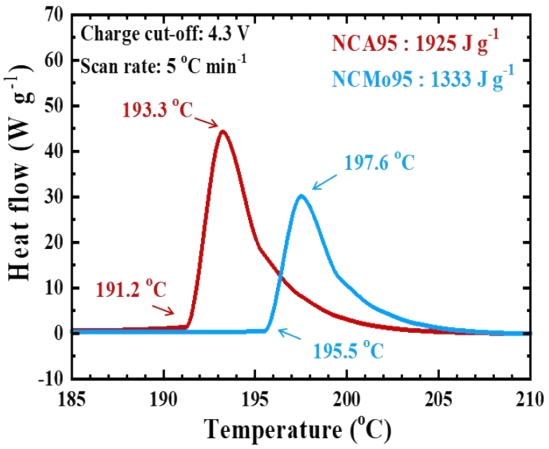

Fig. S19. DSC results of NCA95 and NCMo95 cathodes charged to 4.3 V. The cathodes were lithiated at 700 °C for 10 h.

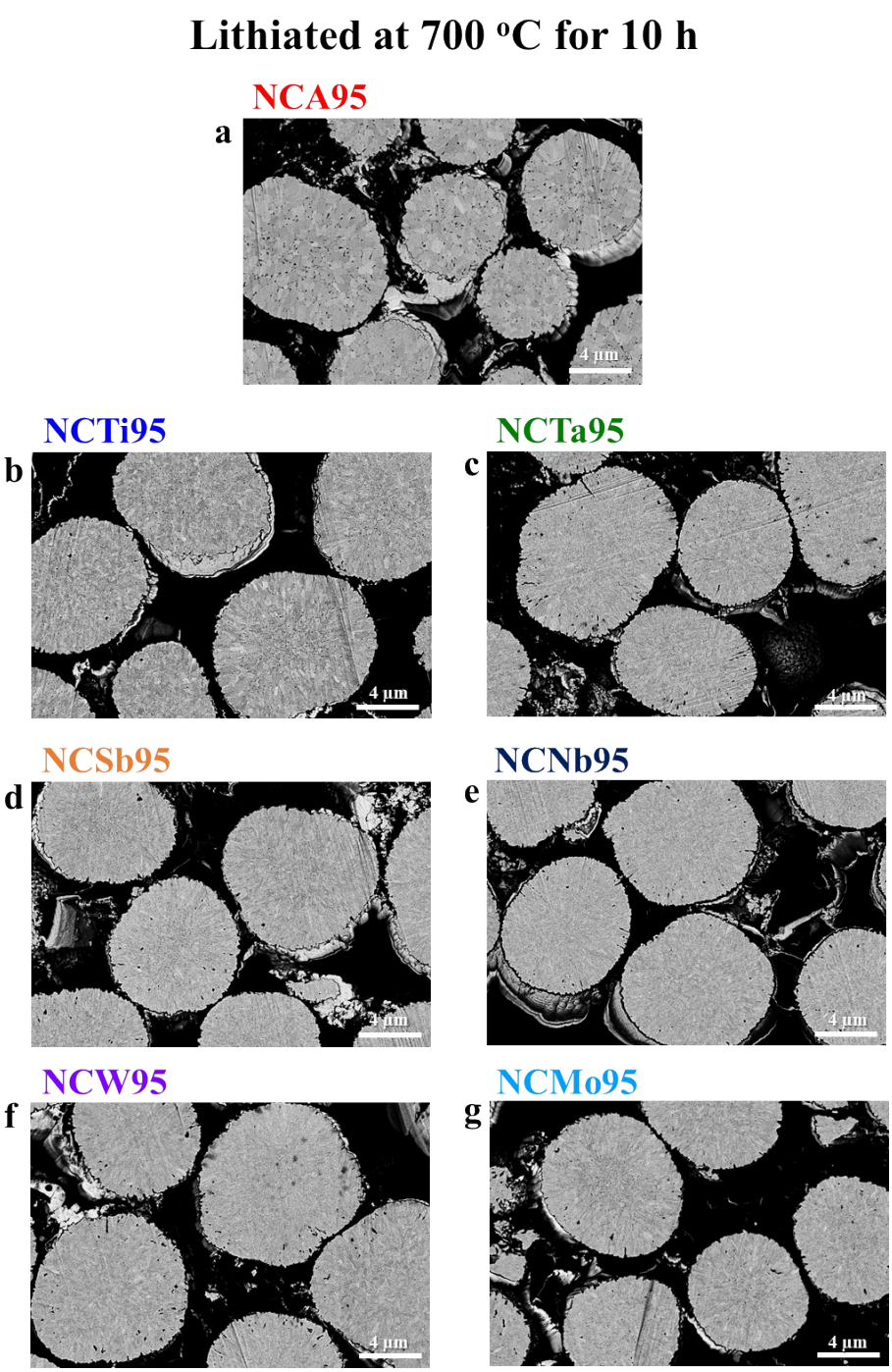

Fig. S20. Low-magnification cross-sectional SEM images of (a) NCA95, (b) NCTi95, (c) NCTa95, (d) NCSb95, (e) NCNb95, (f) NCW95, and (g) NCMo95 cathodes lithiated at 700 °C for 10 h.

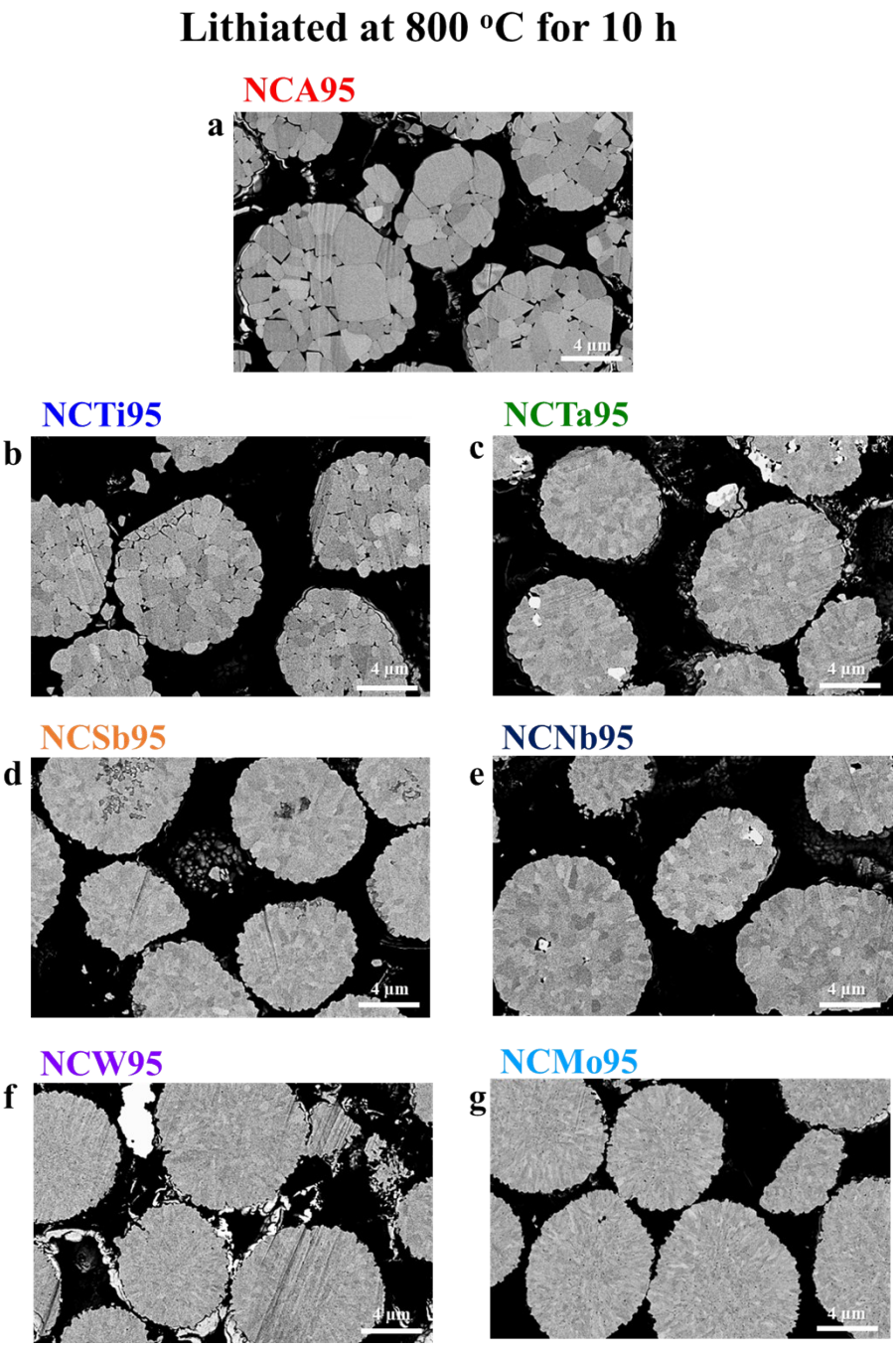

Fig. S21. Low-magnification cross-sectional SEM images of (a) NCA95, (b) NCTi95, (c) NCTa95, (d) NCSb95, (e) NCNb95, (f) NCW95, and (g) NCMo95 cathodes lithiated at 800 °C for 10 h.

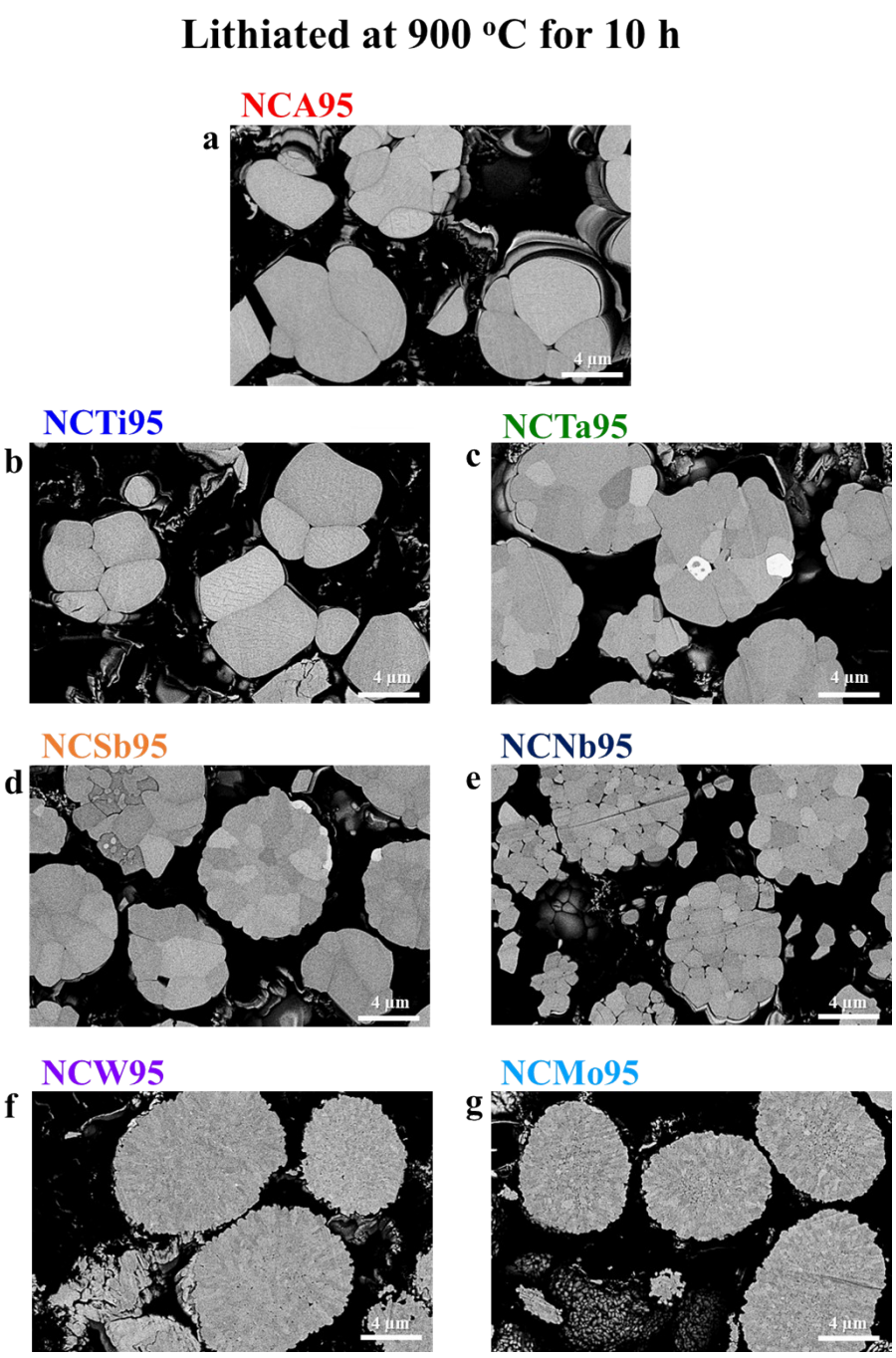

Fig. S22. Low-magnification cross-sectional SEM images of (a) NCA95, (b) NCTi95, (c) NCTa95, (d) NCSb95, (e) NCNb95, (f) NCW95, and (g) NCMo95 cathodes lithiated at 900 °C for 10 h.

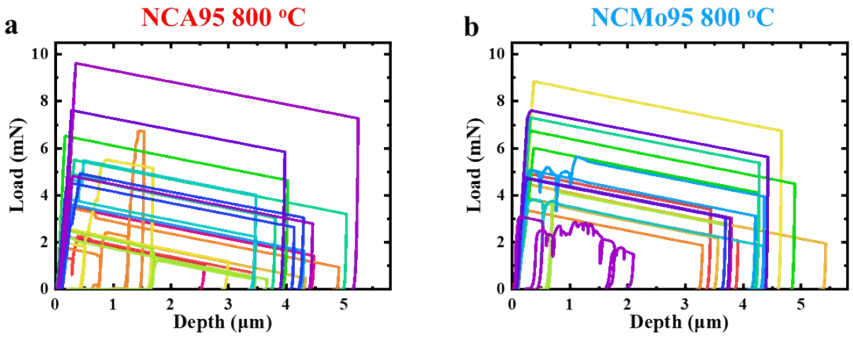

Fig. S23. Load-displacement curves of (a) NCA95, and (b) NCMo95 cathode particles lithiated at 800 °C for 10 h.

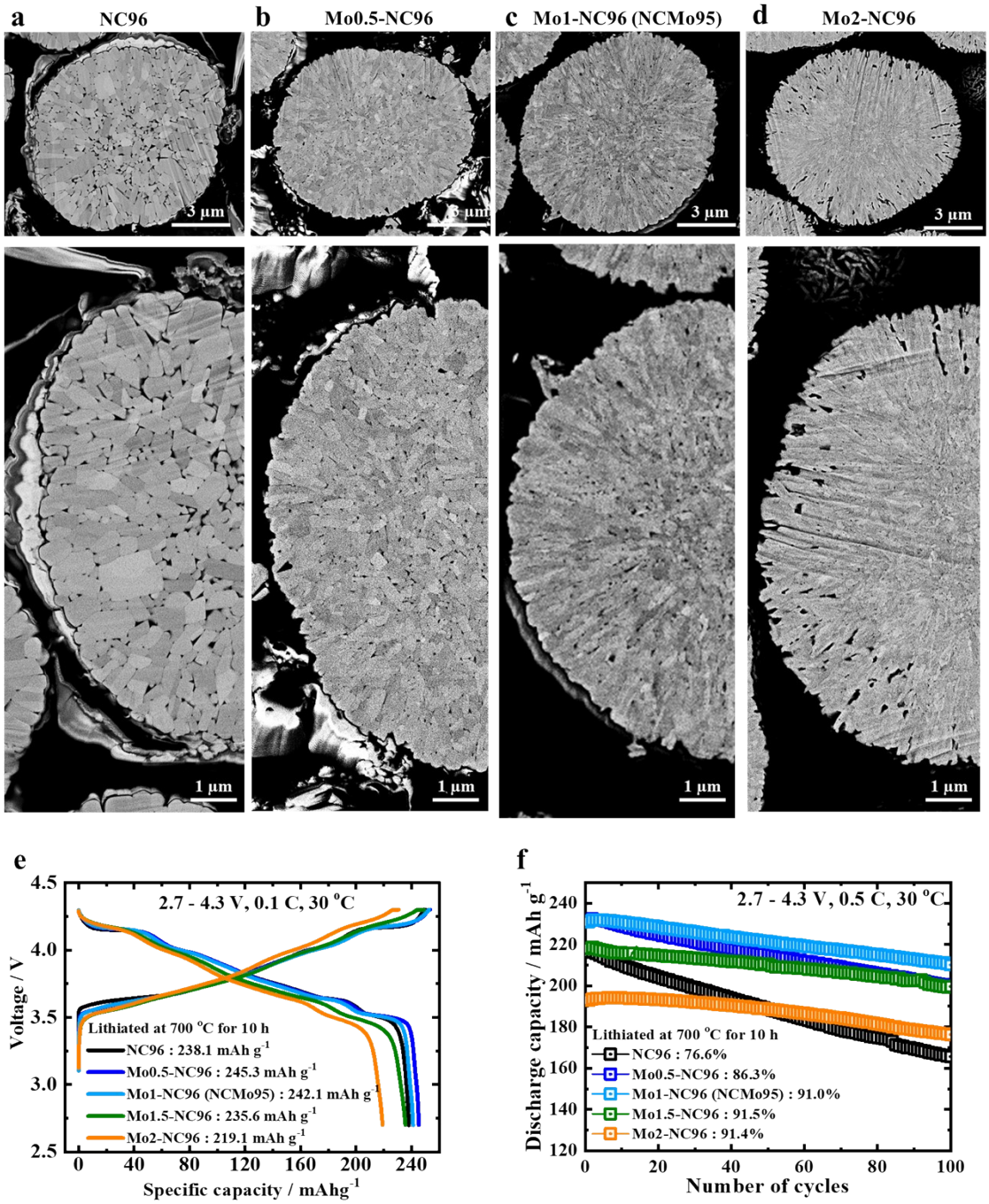

Fig. S24. Cross-sectional SEM images of (a) NC96, (b) Mo0.5-NC96, (c) Mo1-NC96, and (d) Mo2-NC96 cathodes. (e) Initial charge–discharge characteristics and (f) cycling performance of half-cells featuring a series of Mo-doped NC96 cathodes lithiated at 700 °C for 10 h.

Table S1. Chemical compositions of NCA95 and NCMo95 cathode powders lithiated at 700 °C for 10, 20, 30, and 60 h, as determined by ICP-OES.

Sample	Lithiation temperature	Lithiation time	Ni (at%)	Co (at%)	Al (at%)	Mo (at%)
NCA95	700 °C	10 h	95.04	3.91	1.05	-
		20 h	94.94	3.99	1.07	-
		30 h	95.11	3.92	0.97	-
		60 h	95.02	3.96	1.02	-
NCMo95		10 h	95.14	3.89	-	0.97
		20 h	95.13	3.92	-	0.95
		30 h	95.1	3.91	-	0.99
		60 h	95.04	3.94	-	1.02

Table S2. Structural parameters determined by Rietveld refinement of the X-ray diffraction data of NCA95 cathodes lithiated at 700 °C for 10, 20, 30, and 60 h.

$Li[Ni_{0.95}Co_{0.04}Al_{0.01}]O_2$		Space group : $R\bar{3}m$		Lithiated for 10 h		
a-axis: 2.8726 (1) Å		*c*-axis: 14.1896 (2) Å		Volume: 101.403 (1) Å^3		
R_p: 2.81%	R_{wp}: 3.21%	R_{exp}: 2.11%	Chi^2: 3.12			
Atom	Wyckoff position	x	y	z	B_{iso}	*Modified occupancy
Li1	3a	0	0	0	1.200	0.987
Ni2	3a	0	0	0	1.200	0.013
Ni1	3b	0	0	0.5	0.5050	0.937
Co1	3b	0	0	0.5	0.5050	[a]0.040
Al1	3b	0	0	0.5	0.5050	[a]0.010
Li2	3b	0	0	0.5	0.5050	0.013
O1	6c	0	0	0.2417 (2)	0.7750	2

$Li[Ni_{0.95}Co_{0.04}Al_{0.01}]O_2$		Space group : $R\bar{3}m$		Lithiated for 20 h		
a-axis: 2.8729 (2) Å		*c*-axis: 14.1885 (1) Å		Volume: 101.416 (4) Å^3		
R_p: 2.77%	R_{wp}: 3.27%	R_{exp}: 2.12%	Chi^2: 3.11			
Atom	Wyckoff position	x	y	z	B_{iso}	*Modified occupancy
Li1	3a	0	0	0	1.200	0.990
Ni2	3a	0	0	0	1.200	0.010
Ni1	3b	0	0	0.5	0.5050	0.940
Co1	3b	0	0	0.5	0.5050	[a]0.040
Al1	3b	0	0	0.5	0.5050	[a]0.010
Li2	3b	0	0	0.5	0.5050	0.010
O1	6c	0	0	0.2417 (1)	0.7750	2

$Li[Ni_{0.95}Co_{0.04}Al_{0.01}]O_2$		Space group : $R\bar{3}m$		Lithiated for 30 h		
a-axis: 2.8734 (3) Å		*c*-axis: 14.1871 (1) Å		Volume: 101.442 (4) Å^3		
R_p: 2.75%	R_{wp}: 3.41%	R_{exp}: 2.11%	Chi^2: 3.11			
Atom	Wyckoff position	x	y	z	B_{iso}	*Modified occupancy
Li1	3a	0	0	0	1.200	0.993
Ni2	3a	0	0	0	1.200	0.007
Ni1	3b	0	0	0.5	0.5050	0.943
Co1	3b	0	0	0.5	0.5050	[a)]0.040
Al1	3b	0	0	0.5	0.5050	[a)]0.010
Li2	3b	0	0	0.5	0.5050	0.007
O1	6c	0	0	0.2411 (3)	0.7750	2

1

$Li[Ni_{0.95}Co_{0.04}Al_{0.01}]O_2$		Space group : $R\bar{3}m$		Lithiated for 60 h		
a-axis: 2.8737 (1) Å		*c*-axis: 14.1863 (2) Å		Volume: 101.457 (1) Å^3		
R_p: 2.71%	R_{wp}: 3.33%	R_{exp}: 2.11%	Chi^2: 3.11			
Atom	Wyckoff position	x	y	z	B_{iso}	*Modified occupancy
Li1	3a	0	0	0	1.200	0.992
Ni2	3a	0	0	0	1.200	0.008
Ni1	3b	0	0	0.5	0.5050	0.942
Co1	3b	0	0	0.5	0.5050	[a)]0.040
Al1	3b	0	0	0.5	0.5050	[a)]0.010
Li2	3b	0	0	0.5	0.5050	0.008
O1	6c	0	0	0.2418 (1)	0.7750	2

2 *Modified occ. = occupation *12 for Fullprof (occ.*12)

3 [a)] Fixed value

5
4

Table S3. Structural parameters determined by Rietveld refinement of the X-ray diffraction data of NCMo95 cathodes lithiated at 700 °C for 10, 20, 30, and 60 h.

$Li[Ni_{0.95}Co_{0.04}Mo_{0.01}]O_2$		Space group : $R\bar{3}m$		Lithiated for 10 h		
a-axis: 2.8751 (3) Å		*c*-axis: 14.1985 (1) Å		Volume: 101.643 (4) Å^3		
R_p: 3.33%	R_{wp}: 4.27%	R_{exp}: 3.45%	Chi^2: 1.53			
Atom	Wyckoff position	x	y	z	B_{iso}	*Modified occupancy
Li1	3a	0	0	0	1.200	0.976
Ni2	3a	0	0	0	1.200	0.024
Ni1	3b	0	0	0.5	0.5050	0.926
Co1	3b	0	0	0.5	0.5050	[a)]0.040
Mo1	3b	0	0	0.5	0.5050	[a)]0.010
Li2	3b	0	0	0.5	0.5050	0.024
O1	6c	0	0	0.2419 (1)	0.7750	2

$Li[Ni_{0.95}Co_{0.04}Mo_{0.01}]O_2$		Space group : $R\bar{3}m$		Lithiated for 20 h		
a-axis: 2.8756 (1) Å		*c*-axis: 14.1927 (1) Å		Volume: 101.637 (2) Å^3		
R_p: 3.27%	R_{wp}: 4.24%	R_{exp}: 3.37%	Chi^2: 1.51			
Atom	Wyckoff position	x	y	z	B_{iso}	*Modified occupancy
Li1	3a	0	0	0	1.200	0.977
Ni2	3a	0	0	0	1.200	0.023
Ni1	3b	0	0	0.5	0.5050	0.927
Co1	3b	0	0	0.5	0.5050	[a)]0.040
Mo1	3b	0	0	0.5	0.5050	[a)]0.010
Li2	3b	0	0	0.5	0.5050	0.023
O1	6c	0	0	0.2419 (2)	0.7750	2

$Li[Ni_{0.95}Co_{0.04}Mo_{0.01}]O_2$		Space group : $R\bar{3}m$		Lithiated for 30 h		
a-axis: 2.8759 (2) Å		*c*-axis: 14.1889 (1) Å		Volume: 101.631 (2) Å^3		
R_p: 2.61%	R_{wp}: 3.48%	R_{exp}: 2.19%	Chi^2: 2.52			
Atom	Wyckoff position	x	y	z	B_{iso}	*Modified occupancy
Li1	3a	0	0	0	1.200	0.978
Ni2	3a	0	0	0	1.200	0.022
Ni1	3b	0	0	0.5	0.5050	0.928
Co1	3b	0	0	0.5	0.5050	[a)]0.040
Mo1	3b	0	0	0.5	0.5050	[a)]0.010
Li2	3b	0	0	0.5	0.5050	0.022
O1	6c	0	0	0.2419 (4)	0.7750	2

1

$Li[Ni_{0.95}Co_{0.04}Mo_{0.01}]O_2$		Space group : $R\bar{3}m$		Lithiated for 60 h		
a-axis: 2.8761 (3) Å		*c*-axis: 14.1861 (1) Å		Volume: 101.625 (2) Å^3		
R_p: 2.81%	R_{wp}: 3.72%	R_{exp}: 3.11%	Chi^2: 1.64			
Atom	Wyckoff position	x	y	z	B_{iso}	*Modified occupancy
Li1	3a	0	0	0	1.200	0.978
Ni2	3a	0	0	0	1.200	0.022
Ni1	3b	0	0	0.5	0.5050	0.928
Co1	3b	0	0	0.5	0.5050	[a)]0.040
Mo1	3b	0	0	0.5	0.5050	[a)]0.010
Li2	3b	0	0	0.5	0.5050	0.022
O1	6c	0	0	0.2419 (4)	0.7750	2

2 *Modified occ. = occupation *12 for Fullprof (occ.*12)

3 [a)] Fixed value